A functional renormalization group approach to the Anderson impurity model

2009 J. Phys.: Condens. Matter 21 305602

(http://iopscience.iop.org/0953-8984/21/30/305602)

J. Phys.: Condens. Matter **21** (2009) 305602 (14pp) doi:10.1088/0953-8984/21/30/305602

A functional renormalization group approach to the Anderson impurity model

Lorenz Bartosch[1], **Hermann Freire**[1,2], **Jose Juan Ramos Cardenas**[1,3] **and Peter Kopietz**[1]

[1] Institut für Theoretische Physik, Universität Frankfurt, Max-von-Laue Strasse 1, 60438 Frankfurt, Germany
[2] Instituto de Física, Universidade Federal de Goiás, 74.001-970, Goiânia-GO, Brazil
[3] Departamento Fisico-Matematico, Universidad Autonoma de San Luis Potosi, Niño Artillero 140, 78290 San Luis Potosi, Mexico

Received 17 February 2009, in final form 22 May 2009
Published 8 July 2009
Online at stacks.iop.org/JPhysCM/21/305602

Abstract

We develop a functional renormalization group approach which describes the low-energy single-particle properties of the Anderson impurity model up to intermediate on-site interactions $U \lesssim 15\Delta$, where Δ is the hybridization in the wide-band limit. Our method is based on a generalization of a method proposed by Schütz *et al* (2005 *Phys. Rev.* B **72** 035107), using two independent Hubbard–Stratonovich fields associated with transverse and longitudinal spin fluctuations. Although we do not reproduce the exponentially small Kondo scale in the limit $U \to \infty$, the spin fluctuations included in our approach remove the unphysical Stoner instability predicted by mean field theory for $U > \pi\Delta$. We discuss different decoupling schemes and show that a decoupling which manifestly respects the spin-rotational invariance of the problem gives rise to the lowest quasiparticle weight. To obtain a closed flow equation for the fermionic self-energy we also propose a new scheme of truncation of the functional renormalization group flow equations using Dyson–Schwinger equations to express bosonic vertex functions in terms of fermionic ones.

(Some figures in this article are in colour only in the electronic version)

1. Introduction

The Anderson impurity model (AIM) is one of the most important model systems in condensed matter physics [1]. The model was originally proposed by Anderson [2] to describe the properties of local moments in metals. Its Hamiltonian describes a single correlated impurity which is coupled to a band of non-interacting conduction electrons,

$$\hat{H} = \sum_{k\sigma}(\epsilon_k - \sigma h)\hat{c}^\dagger_{k\sigma}\hat{c}_{k\sigma} + \sum_{\sigma}(E_{\rm d} - \sigma h)\hat{d}^\dagger_\sigma\hat{d}_\sigma + U\hat{d}^\dagger_\uparrow\hat{d}_\uparrow\hat{d}^\dagger_\downarrow\hat{d}_\downarrow + \sum_{k\sigma}(V^*_k\hat{d}^\dagger_\sigma\hat{c}_{k\sigma} + V_k\hat{c}^\dagger_{k\sigma}\hat{d}_\sigma). \quad (1.1)$$

Here, $\hat{c}_{k\sigma}$ annihilates a non-interacting conduction electron with momentum k, energy dispersion ϵ_k and spin projection σ, while the operator $\hat{d}_\sigma$ annihilates a localized correlated d electron with atomic energy $E_{\rm d}$ and on-site repulsion U. The hybridization between the d electrons and the conduction electrons is characterized by the hybridization energy V_k. We have also included in equation (1.1) the Zeeman energy h associated with an external magnetic field.

The thermodynamic and spectral properties of the AIM can be calculated accurately by means of Wilson's numerical renormalization group [3–5] (NRG); see [6] for a recent review. However, the calculation of the spectral function $A(\omega)$ of the d electrons by means of the NRG requires some computational effort, in particular if one needs accurate results for arbitrary frequencies ω. Since the quantitative knowledge of the spectral function of the AIM for all ω is essential in the context of the dynamical mean field theory describing strong correlations in realistic three-dimensional fermion systems [7], it is important to develop approximate analytical methods for calculating the spectral function of the AIM. Although several analytical approaches have been proposed for describing the strong coupling regime [8–14], a satisfactory analytical alternative which can compete with the NRG in the strong coupling regime has not been found. This has motivated us to develop

a new functional renormalization group (FRG) approach to the AIM which is not based on the weak coupling truncation used by other authors [15, 16]. Our approach extends the collective field FRG developed in [17–19], which is based on the partial bosonization of the two-body interaction using suitable Hubbard–Stratonovich fields. For simplicity, we focus here on the local moment regime [1], where the energy $E_{\rm d}$ of the d level is located below the Fermi energy, but its double occupancy is prohibited by a strong on-site interaction U. In the limit $U \to \infty$ the low-energy properties of the AIM are in this regime identical to those of the Kondo model describing only the spin degree of freedom of the impurity. It is then natural to decouple the interaction of the AIM in terms of Hubbard–Stratonovich fields representing collective spin fluctuations, which should be treated non-perturbatively to describe the strong coupling regime.

Since we are interested in the correlation functions of the d electrons, we simply integrate out the conduction electrons using the coherent state functional integral. The ratio of the partition functions with and without interaction at constant chemical potential μ and inverse temperature β can then be written as

$$\frac{\mathcal{Z}}{\mathcal{Z}_0} = \frac{\int \mathcal{D}[d,\bar{d}]\mathrm{e}^{-S_0[\bar{d},d]-S_U[\bar{d},d]}}{\int \mathcal{D}[d,\bar{d}]\mathrm{e}^{-S_0[\bar{d},d]}}, \tag{1.2}$$

where the Gaussian part is given by

$$\begin{aligned} S_0[\bar{d},d] &= \int_0^\beta \mathrm{d}\tau \sum_\sigma \bar{d}_\sigma(\tau)\left[\partial_\tau + E_{\rm d} - \mu - \sigma h\right] d_\sigma(\tau) \\ &\quad + \int_0^\beta \mathrm{d}\tau \int_0^\beta \mathrm{d}\tau' \sum_\sigma \bar{d}_\sigma(\tau)\Delta^\sigma(\tau-\tau')d_\sigma(\tau') \\ &= -\int_\omega \sum_\sigma [\mathrm{i}\omega - \xi_0^\sigma - \Delta^\sigma(\mathrm{i}\omega)]\bar{d}_{\omega\sigma} d_{\omega\sigma}, \end{aligned} \tag{1.3}$$

with

$$\xi_0^\sigma = E_{\rm d} - \mu - \sigma h, \tag{1.4}$$

and the interaction is

$$S_U[\bar{d},d] = U\int_0^\beta \mathrm{d}\tau \bar{d}_\uparrow(\tau)d_\uparrow(\tau)\bar{d}_\downarrow(\tau)d_\downarrow(\tau). \tag{1.5}$$

Here, $\int_\omega = \frac{1}{\beta}\sum_\omega$ denotes summation over fermionic Matsubara frequencies. Later we shall take the limit $\beta \to \infty$ where $\int_\omega = \int \frac{\mathrm{d}\omega}{2\pi}$. The Fourier transform of the Grassmann fields $d_\sigma(\tau)$ in frequency space is defined by

$$d_\sigma(\tau) = \int_\omega \mathrm{e}^{-\mathrm{i}\omega\tau}\, \mathrm{d}_{\omega\sigma}, \tag{1.6}$$

and the hybridization function is

$$\Delta^\sigma(\tau) = \int_\omega \mathrm{e}^{-\mathrm{i}\omega\tau}\Delta^\sigma(\mathrm{i}\omega), \tag{1.7}$$

with Fourier components

$$\Delta^\sigma(\mathrm{i}\omega) = \sum_k \frac{|V_k|^2}{\mathrm{i}\omega - \epsilon_k + \mu + \sigma h}. \tag{1.8}$$

The 0 + 1-dimensional quantum field theory defined in equations (1.3)–(1.5) will be the starting point of our further calculations presented below.

Let us briefly outline the rest of this work. In section 2 we decouple the interaction (1.5) in the spin-singlet particle–hole channel using a complex Hubbard–Stratonovich field which describes transverse spin-flip fluctuations. By treating the resulting field theory on the level of the Gaussian approximation, we obtain results for the dynamic structure factor and the self-energy in the ladder approximation. Of course, only for small U can we expect the ladder approximation to give reliable results. For larger couplings we find a ferromagnetic Stoner instability, consistent with the Hartree–Fock approximation but in contrast to well-established results. To go beyond the simple ladder approximation, we use in section 3 a collective field FRG approach for our Bose–Fermi theory and implement a simple truncation to close the set of flow equations. Our inclusion of transverse spin fluctuations based on the FRG removes the unphysical Stoner instability and gives results which qualitatively describe the correct physics. However, although the quasiparticle weight vanishes with increasing interaction as it should, it does not obey the well-known Kondo scaling. To improve on these results, we introduce in section 4 a new FRG approach with partial bosonization in both the transverse and the longitudinal channel. We discuss the ambiguities with the distribution of weight among the two channels and show that in the manifestly spin-rotationally invariant case we get the strongest suppression of the quasiparticle weight. Finally, in section 5 we summarize our results and discuss some open questions.

2. Ladder approximation in the spin-singlet particle–hole channel

2.1. Hartree–Fock approximation and Stoner instability

If we treat the interaction (1.5) within the self-consistent Hartree–Fock approximation, we obtain the renormalized excitation energy $\xi^\sigma = \xi_0^\sigma + \delta\xi^\sigma$, with

$$\delta\xi^\sigma = U\int_\omega G_0^{\bar{\sigma}}(\mathrm{i}\omega), \tag{2.1}$$

where we have used the notation $\bar{\sigma} = -\sigma$ for the spin label. The self-consistent Hartree–Fock Green function is

$$G_0^\sigma(\mathrm{i}\omega) = \frac{1}{\mathrm{i}\omega - \xi^\sigma - \Delta^\sigma(\mathrm{i}\omega)}. \tag{2.2}$$

The corresponding self-energy can be written as

$$\delta\xi^\sigma = \frac{U}{2}[n - \sigma m], \tag{2.3}$$

where $n = n_\uparrow + n_\downarrow$ is the average occupation and $m = n_\uparrow - n_\downarrow$ is the average magnetization of the impurity level. For a sufficiently strong interaction, Hartree–Fock theory predicts a finite value of m even for $h \to 0$. In the wide-band limit, where the hybridization function can be approximated by

$$\Delta^\sigma(\mathrm{i}\omega) = -\mathrm{i}\Delta^\sigma \operatorname{sgn}\omega, \tag{2.4}$$

the Hartree–Fock self-consistency equation for the moment m can be evaluated analytically at zero temperature. For $h = 0$ (where $\Delta^\sigma = \Delta$ is independent of the spin projection) and in the particle–hole symmetric case (where $E_\mathrm{d} - \mu = -U/2$ and $n = 1$) the result is

$$m = \int_\omega \sum_\sigma \sigma G_0^\sigma(\mathrm{i}\omega) = \frac{2}{\pi} \arctan\left(\frac{Um}{2\Delta}\right). \tag{2.5}$$

This equation has a ferromagnetic solution ($m \neq 0$) if

$$u_0 \equiv \frac{U}{\pi\Delta} > 1. \tag{2.6}$$

This ferromagnetic Stoner instability is an artifact of the Hartree–Fock approximation [1], which should be removed once fluctuation corrections are properly taken into account.

2.2. Hubbard–Stratonovich transformation in the spin-singlet particle–hole channel

The best decoupling of the electron–electron interaction in a given model is always a very delicate question and requires, *a priori*, physical insight about the model. Therefore, the choice of the decoupling must always be motivated physically. In the strong coupling limit we expect the transverse spin fluctuations to play an important role in removing the Stoner instability [11]. It is therefore natural to decouple the interaction in the spin-singlet particle–hole channel with the help of a bosonic Hubbard–Stratonovich field, describing transverse spin fluctuations. To this end, we use the antisymmetry of the Grassmann fields to write the integrand in the interaction functional (1.5) as

$$U\bar{d}_\uparrow d_\uparrow \bar{d}_\downarrow d_\downarrow = -U(\bar{d}_\uparrow d_\downarrow)(\bar{d}_\downarrow d_\uparrow) = -U\bar{s}(\tau)s(\tau), \tag{2.7}$$

where we have defined the composite spin-flip fields,

$$\bar{s}(\tau) = \bar{d}_\uparrow(\tau)d_\downarrow(\tau), \qquad s(\tau) = \bar{d}_\downarrow(\tau)d_\uparrow(\tau). \tag{2.8}$$

Introducing the complex bosonic Hubbard–Stratonovich fields $\chi(\tau)$ and $\bar{\chi}(\tau)$ conjugate to $\bar{s}(\tau)$ and $s(\tau)$, the ratio (1.2) can be written as a functional integral over a six-component superfield $\Phi = [d_\uparrow, \bar{d}_\uparrow, d_\downarrow, \bar{d}_\downarrow, \chi, \bar{\chi}]$,

$$\frac{\mathcal{Z}}{\mathcal{Z}_\mathrm{HF}} = \frac{\int \mathcal{D}[\Phi]\mathrm{e}^{-S_0[\Phi]-S_1[\Phi]}}{\int \mathcal{D}[\Phi]\mathrm{e}^{-S_0[\Phi]}}, \tag{2.9}$$

where $\mathcal{Z}_\mathrm{HF}$ is the partition function in Hartree–Fock approximation. The Gaussian part of the bare action is

$$S_0[\Phi] = -\int_\omega \sum_\sigma \left[G_0^\sigma(\mathrm{i}\omega)\right]^{-1} \bar{d}_{\omega\sigma} d_{\omega\sigma} + \int_{\bar{\omega}} U^{-1}\bar{\chi}_{\bar{\omega}}\chi_{\bar{\omega}}, \tag{2.10}$$

and the interaction part can be written as

$$S_1[\Phi] = \int_{\bar{\omega}} [\bar{s}_{\bar{\omega}}\chi_{\bar{\omega}} + s_{\bar{\omega}}\bar{\chi}_{\bar{\omega}}] - \int_\omega \sum_\sigma \delta\xi^\sigma \bar{d}_{\omega\sigma} d_{\omega\sigma}, \tag{2.11}$$

where

$$s_{\bar{\omega}} = \int_0^\beta \mathrm{d}\tau \mathrm{e}^{\mathrm{i}\bar{\omega}\tau} s(\tau) = \int_\omega \bar{d}_{\omega\downarrow} d_{\omega+\bar{\omega},\uparrow}, \tag{2.12}$$

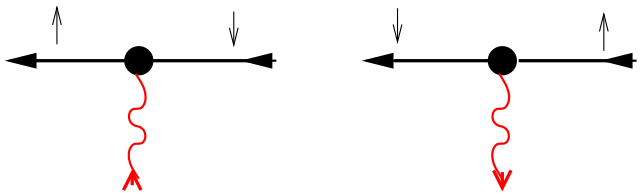

Figure 1. Graphical representation of the bare boson–fermion vertices of the action $S_1[\Phi]$ in equation (2.11). Solid arrows pointing into the vertices represent d_σ, while outgoing solid arrows represent $\bar{d}_\sigma$. The small arrows indicate the spin projections. The wavy arrows represent the spin-flip field χ (pointing into the black dots) and $\bar{\chi}$ (pointing out of the black dots). The direction of the arrows associated with the wavy lines is chosen such that the incoming arrow adds spin to the vertex.

$$\bar{s}_{\bar{\omega}} = \int_0^\beta \mathrm{d}\tau \mathrm{e}^{-\mathrm{i}\bar{\omega}\tau} \bar{s}(\tau) = \int_\omega \bar{d}_{\omega+\bar{\omega},\uparrow} d_{\omega\downarrow}. \tag{2.13}$$

Because $[G_0^\sigma(\mathrm{i}\omega)]^{-1}$ in the Gaussian part (2.10) of the action is by definition the inverse Hartree–Fock Green function (2.2), the Hartree–Fock self-energy $\delta\xi^\sigma$ should be subtracted from the interaction in equation (2.11) as a counterterm. The boson–fermion interaction in equation (2.11) can be written as

$$\begin{aligned}\int_{\bar{\omega}} &[\bar{s}_{\bar{\omega}}\chi_{\bar{\omega}} + s_{\bar{\omega}}\bar{\chi}_{\bar{\omega}}] \\ &= \int_{\bar{\omega}}\int_\omega [\Gamma_0^{(\bar{d}_\uparrow d_\downarrow \chi)}(\omega+\bar{\omega}, \omega, \bar{\omega})\bar{d}_{\omega+\bar{\omega}\uparrow} d_{\omega\downarrow}\chi_{\bar{\omega}} \\ &\quad + \Gamma_0^{(\bar{d}_\downarrow d_\uparrow \bar{\chi})}(\omega-\bar{\omega}, \omega, \bar{\omega})\bar{d}_{\omega-\bar{\omega}\downarrow} d_{\omega\uparrow}\bar{\chi}_{\bar{\omega}}],\end{aligned} \tag{2.14}$$

with the bare spin-flip vertices given by

$$\Gamma_0^{(\bar{d}_\uparrow d_\downarrow \chi)}(\omega+\bar{\omega}, \omega, \bar{\omega}) = \Gamma_0^{(\bar{d}_\downarrow d_\uparrow \bar{\chi})}(\omega-\bar{\omega}, \omega, \bar{\omega}) = 1. \tag{2.15}$$

A graphical representation of these vertices is shown in figure 1.

2.3. Gaussian propagator of transverse spin fluctuations

If we integrate in equation (2.9) over the fermion fields, we obtain the effective action $S_\mathrm{eff}[\bar{\chi}, \chi]$ of the spin-flip fields $\chi, \bar{\chi}$. Expanding $S_\mathrm{eff}[\bar{\chi}, \chi]$ to quadratic order in the fields (Gaussian approximation), we obtain

$$S_\mathrm{eff}[\bar{\chi}, \chi] \approx \int_{\bar{\omega}} [F_\mathrm{LA}^\perp(\mathrm{i}\bar{\omega})]^{-1} \bar{\chi}_{\bar{\omega}}\chi_{\bar{\omega}}. \tag{2.16}$$

The inverse spin-flip propagator in ladder approximation (LA) is given by

$$[F_\mathrm{LA}^\perp(\mathrm{i}\bar{\omega})]^{-1} = U^{-1} - \Pi_0^\perp(\mathrm{i}\bar{\omega}), \tag{2.17}$$

where $\Pi_0^\perp(\mathrm{i}\bar{\omega})$ is the non-interacting dynamic spin-flip susceptibility

$$\Pi_0^\perp(\mathrm{i}\bar{\omega}) = -\int_\omega G_0^\uparrow(\mathrm{i}\omega) G_0^\downarrow(\mathrm{i}\omega - \mathrm{i}\bar{\omega}). \tag{2.18}$$

In the wide-band limit, where $\Delta^\sigma(\mathrm{i}\omega)$ is given by equation (2.4), the integration in equation (2.18) can be

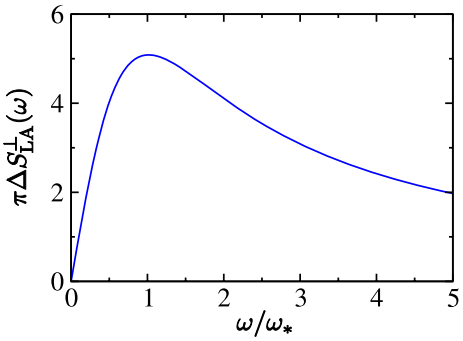

Figure 2. Graph of the transverse spin structure factor $S^{\perp}_{\rm LA}(\omega)$ in ladder approximation for $h = 0$, $u_0 = U/(\pi\Delta) = 0.9$ and particle–hole symmetry. The characteristic energy scale of transverse spin fluctuations is in this approximation given by $\omega_* \approx \Delta(1 - u_0)$.

performed analytically at zero temperature. In this work we only need $\Pi^{\perp}_0(\mathrm{i}\bar{\omega})$ in the absence of an external magnetic field and spontaneous ferromagnetism, where $\xi^{\sigma} = \xi$ and $\Delta^{\sigma} = \Delta$ are independent of the spin projection σ,

$$\Pi^{\perp}_0(\mathrm{i}\bar{\omega}) = \frac{\Delta}{\pi|\bar{\omega}|(|\bar{\omega}| + 2\Delta)} \ln\left[\frac{\xi^2 + (|\bar{\omega}| + \Delta)^2}{\xi^2 + \Delta^2}\right]. \quad (2.19)$$

If we assume in addition particle–hole symmetry so that $\xi = \xi_0 + \delta\xi = 0$, then equation (2.19) further simplifies to

$$\pi\Delta\Pi^{\perp}_0(\mathrm{i}\bar{\omega}) = \frac{\ln[1 + |\bar{\epsilon}|]}{|\bar{\epsilon}|(1 + |\bar{\epsilon}|/2)} = 1 - |\bar{\epsilon}| + \frac{5}{6}\bar{\epsilon}^2 + \mathcal{O}(|\bar{\epsilon}|^3), \quad (2.20)$$

where $\bar{\epsilon} = \bar{\omega}/\Delta$. Within the LA the spectral density $S^{\perp}_{\rm LA}(\omega)$ of transverse spin fluctuations (the dynamic structure factor) is then given by

$$\Pi^{\perp}_{\rm LA}(\mathrm{i}\bar{\omega}) = \frac{\Pi^{\perp}_0(\mathrm{i}\bar{\omega})}{1 - U\Pi^{\perp}_0(\mathrm{i}\bar{\omega})} = \int_0^{\infty} \frac{\mathrm{d}\omega}{\pi} S^{\perp}_{\rm LA}(\omega) \frac{2\omega}{\omega^2 + \bar{\omega}^2}, \quad (2.21)$$

or, equivalently,

$$\mathrm{Im}\,\Pi^{\perp}_{\rm LA}(\omega + \mathrm{i}0) = \mathrm{sgn}\,\omega S^{\perp}_{\rm LA}(|\omega|). \quad (2.22)$$

A graph of $S^{\perp}_{\rm LA}(\omega)$ for $u_0 = U/(\pi\Delta) = 0.9$ is shown in figure 2. In the regime $0 < 1 - u_0 \ll 1$ the LA predicts a well-defined peak in the dynamic structure factor at the energy scale

$$\omega_* = \Delta(1 - u_0). \quad (2.23)$$

The width of the peak is of the order of Δ. In fact, in this regime the low-frequency behavior of $S^{\perp}_{\rm LA}(\omega)$ can easily be obtained analytically. For $|\omega| \ll \Delta$ we find

$$\Pi^{\perp}_{\rm LA}(\mathrm{i}\bar{\omega}) = \frac{1}{\pi} \frac{1}{\omega_* + u_0|\bar{\omega}|}, \quad (2.24)$$

so the corresponding structure factor is

$$S^{\perp}_{\rm LA}(\omega) \approx \frac{1}{\pi} \frac{\omega}{\omega_*^2 + \omega^2}. \quad (2.25)$$

For $u_0 \to 1$ the energy scale ω_* vanishes, indicating an instability towards spontaneous ferromagnetism, as suggested by the Hartree–Fock approximation discussed in section 2.1. Because we know that the AIM does not exhibit spontaneous ferromagnetism for arbitrary values of U, we expect the LA to only be accurate for $u_0 \ll 1$. Before employing more sophisticated FRG methods to include fluctuation corrections which remove this unphysical Stoner instability, it is instructive to consider the d electron self-energy within the LA, which we shall do in section 2.4.

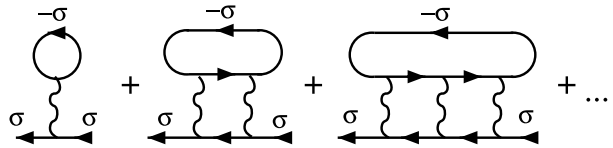

Figure 3. Diagrams contributing to the fermionic self-energy $\Sigma(\mathrm{i}\omega)$ in the particle–hole ladder approximation; see equation (2.26). Solid arrows denote fermionic Hartree–Fock Green functions and wavy lines denote the bare interaction. The first-order (Hartree) diagram is subtracted in equation (2.27).

2.4. Fermionic self-energy in the ladder approximation

The LA in the particle–hole channel gives the following self-energy for the d electrons:

$$\Sigma^{\sigma}(\mathrm{i}\omega) = \int_{\bar{\omega}} F^{\perp}_{\rm LA}(\mathrm{i}\bar{\omega}) G^{\bar{\sigma}}_0(\mathrm{i}\omega - \mathrm{i}\sigma\bar{\omega}). \quad (2.26)$$

The infinite series of Feynman diagrams which is included in equation (2.26) is shown in figure 3. Subtracting the Hartree–Fock correction $\delta\xi^{\sigma}$ given in equation (2.1) which formally arises from the counterterm in equation (2.11), the frequency-dependent part of the self-energy can also be written as

$$\delta\Sigma^{\sigma}(\mathrm{i}\omega) \equiv \Sigma^{\sigma}(\mathrm{i}\omega) - \delta\xi^{\sigma} = U^2 \int_{\bar{\omega}} \Pi^{\perp}_{\rm LA}(\mathrm{i}\bar{\omega}) G^{\bar{\sigma}}_0(\mathrm{i}\omega - \mathrm{i}\sigma\bar{\omega}). \quad (2.27)$$

Of particular interest is the quasiparticle residue Z^{σ}, which is defined by

$$Z^{\sigma} = \frac{1}{1 - \left.\frac{\partial\,\mathrm{Re}\,\Sigma^{\sigma}(\omega + \mathrm{i}0)}{\partial\omega}\right|_{\omega=0}}. \quad (2.28)$$

In figure 4 we show the prediction of the LA for the interaction dependence of the quasiparticle residue in the non-magnetic, particle–hole symmetric case with and without linearization of the spin-flip susceptibility $\Pi^{\perp}_0(\mathrm{i}\bar{\omega})$. Obviously, the linearization of the spin-flip susceptibility does lead to modest changes of the Z-factor. The vanishing of Z at $u_0 = 1$ is an unphysical artifact of the LA, which implicitly contains the Stoner instability via the spin susceptibility. In section 3 we shall show how to remove this instability by including the feedback of the fermionic wavefunction renormalization on the spin susceptibility.

3. FRG with partial bosonization in the spin-singlet particle–hole channel

To go beyond the ladder approximation, we now use the collective field FRG approach developed in [17–19] to study

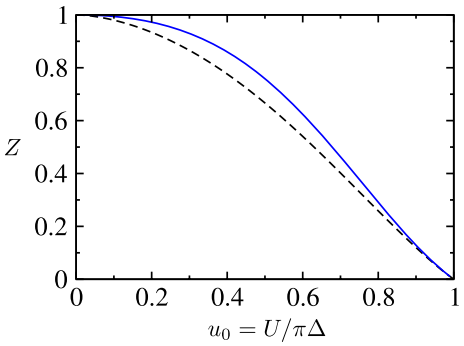

Figure 4. Graph of the quasiparticle residue Z as a function of $u_0 = U/(\pi\Delta)$ within LA for $h = 0$ and particle–hole symmetric filling $E_d - \mu = -\frac{U}{2}$. While in the calculation of the solid line (blue) the full polarization was used, in the calculation of the dashed line (black) we have used the linearized spin susceptibility $\pi\Delta\Pi_0^{\perp}(i\bar{\omega}) \approx 1 - |\bar{\omega}|/\Delta$.

the mixed Bose–Fermi theory defined by the action $S[\Phi] = S_0[\Phi] + S_1[\Phi]$ in equations (2.10) and (2.11). In fact, this theory has a formal similarity with the theory describing two coupled metallic chains, which was studied by means of the FRG in [20]. The exact FRG flow equations in the present problem are therefore represented by the same Feynman diagrams as were given in [20].

3.1. Exact FRG flow equations

To derive exact FRG flow equations, we modify our original model by introducing an ultraviolet cutoff Λ_0 and an infrared cutoff Λ into the Gaussian part (2.10) of the action. In our renormalization group (RG) scheme the infrared cutoff is introduced only in the bosonic sector and is reduced from its initial value $\Lambda = \Lambda_0$ to zero during the RG flow [17–20]. In previous FRG studies of the AIM, fermionic degrees of freedom were directly integrated out and a sharp Matsubara frequency cutoff was employed [15, 16]. For our purpose it is better to work with a smooth cutoff in order to avoid artificial singularities introduced by a sharp cutoff. Formally, we introduce the cutoff via the following substitution in the bosonic part of the Gaussian action $S_0[\Phi]$ given in equation (2.10):

$$U^{-1} \to U^{-1} + R_\Lambda(i\bar{\omega}), \tag{3.1}$$

where

$$R_\Lambda(i\bar{\omega}) = \frac{\Lambda}{\pi\Delta^2} R(|\bar{\omega}|/\Lambda), \tag{3.2}$$

and the function $R(x)$ is given by [21]

$$R(x) = (1-x)\Theta(1-x). \tag{3.3}$$

The flowing spin-flip propagator is then

$$F_\Lambda^{\perp}(i\bar{\omega}) = [U^{-1} - \Pi_\Lambda^{\perp}(i\bar{\omega}) + R_\Lambda(i\bar{\omega})]^{-1} = \frac{U}{1 + U\left[R_\Lambda(i\bar{\omega}) - \Pi_\Lambda^{\perp}(i\bar{\omega})\right]}, \tag{3.4}$$

where $\Pi_\Lambda^{\perp}(i\bar{\omega})$ is the flowing irreducible transverse spin susceptibility. Introducing the corresponding single-scale propagator

$$\dot{F}_\Lambda^{\perp}(i\bar{\omega}) = [-\partial_\Lambda R_\Lambda(i\bar{\omega})][F_\Lambda^{\perp}(i\bar{\omega})]^2, \tag{3.5}$$

the exact FRG flow equation for the irreducible self-energy of spin-σ electrons can then be written as

$$\begin{aligned}\partial_\Lambda \Sigma_\Lambda^{\sigma}(i\omega) = &\int_{\bar{\omega}} \dot{F}_\Lambda^{\perp}(i\bar{\omega}) \Gamma_\Lambda^{(\bar{d}_\sigma d_\sigma \bar{\chi}\chi)}(\omega, \omega; \bar{\omega}, \bar{\omega}) \\ &+ \int_{\bar{\omega}} \dot{F}_\Lambda^{\perp}(i\bar{\omega}) G_\Lambda^{\bar{\sigma}}(i\omega - i\sigma\bar{\omega}) \\ &\times \Gamma_\Lambda^{(\bar{d}_\sigma d_{\bar{\sigma}} \chi_\sigma)}(\omega, \omega - \sigma\bar{\omega}, \sigma\bar{\omega}) \\ &\times \Gamma_\Lambda^{(\bar{d}_{\bar{\sigma}} d_\sigma \chi_{\bar{\sigma}})}(\omega - \sigma\bar{\omega}, \omega, \sigma\bar{\omega}).\end{aligned} \tag{3.6}$$

Here, $\Gamma_\Lambda^{(\bar{d}_\sigma d_\sigma \bar{\chi}\chi)}(\omega, \omega; \bar{\omega}, \bar{\omega})$ is the flowing irreducible vertex with two bosonic and two fermionic external legs, and for the labels of the flowing three-legged boson–fermion vertices we have used the short notation $\chi_\uparrow = \chi$ and $\chi_\downarrow = \bar{\chi}$, so the non-zero combinations are $\Gamma_\Lambda^{(\bar{d}_\uparrow d_\downarrow \chi_\uparrow)}(\omega, \omega - \bar{\omega}, \bar{\omega}) = \Gamma_\Lambda^{(\bar{d}_\uparrow d_\downarrow \chi)}(\omega, \omega - \bar{\omega}, \bar{\omega})$ and $\Gamma_\Lambda^{(\bar{d}_\downarrow d_\uparrow \chi_\downarrow)}(\omega - \bar{\omega}, \omega, \bar{\omega}) = \Gamma_\Lambda^{(\bar{d}_\downarrow d_\uparrow \bar{\chi})}(\omega - \bar{\omega}, \omega, \bar{\omega})$. Actually, the three-legged boson–fermion vertices have the symmetry

$$\Gamma_\Lambda^{(\bar{d}_\downarrow d_\uparrow \bar{\chi})}(\omega - \bar{\omega}, \omega, \bar{\omega}) = \Gamma_\Lambda^{(\bar{d}_\uparrow d_\downarrow \chi)}(\omega, \omega - \bar{\omega}, \bar{\omega}), \tag{3.7}$$

so the two vertices in equation (3.6) have the same value. The flowing d level Green function $G_\Lambda^{\sigma}(i\omega)$ is related to the flowing self-energy via the Dyson equation,

$$G_\Lambda^{\sigma}(i\omega) = \frac{1}{i\omega - \xi_0^{\sigma} - \Delta^{\sigma}(i\omega) - \Sigma_\Lambda^{\sigma}(i\omega)}. \tag{3.8}$$

A graphical representation of the exact FRG flow equation (3.6) is shown in figure 5. The initial values of the boson–fermion vertices are equal to the bare vertices given in equation (2.15), which is unity with our normalization. In principle, the integration of the FRG flow equation (3.6) generates also the Hartree–Fock contribution (2.3) to the self-energy as a boundary term which is of first order in U and

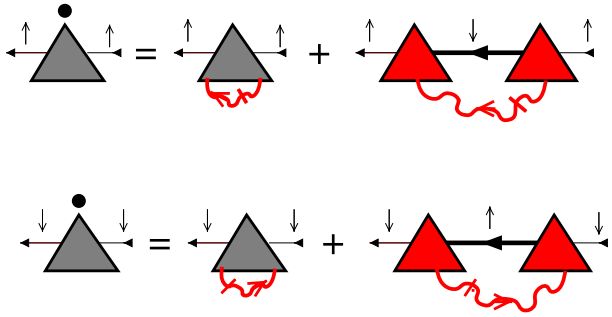

Figure 5. Exact flow equation for the fermionic self-energy $\Sigma_\Lambda^{\sigma}(\omega)$ with Hubbard–Stratonovich decoupling in the spin-singlet particle–hole channel. In our cutoff scheme only the bosonic propagator is regularized via a cutoff. Thick black arrows denote the flowing fermion propagator given in equation (3.8), while thick wavy arrows with a slash denote the flowing single-scale spin-flip propagator defined in equation (3.5). The irreducible vertices are denoted by shaded triangles with the appropriate number of external legs. The dots over the fermionic two-point vertices on the left-hand side represent the derivative with respect to the RG cutoff Λ.

appears when we integrate this equation up to $\Lambda = 0$. In practice, it is better to drop this first-order term and include the Hartree–Fock self-energy from the beginning into the d electron propagator, which amounts to imposing the initial condition

$$\Sigma^{\sigma}_{\Lambda_0}(\mathrm{i}\omega) = \delta\xi^{\sigma} = \frac{U}{2}[n - \sigma m], \tag{3.9}$$

so the initial $G^{\sigma}_{\Lambda_0}(\mathrm{i}\omega)$ is the Hartree–Fock Green function.

3.2. Truncation of the FRG equations via Dyson–Schwinger equations

To obtain a closed system of RG flow equations, we need additional RG equations for the four-legged boson–fermion vertex $\Gamma^{(\bar{d}_\sigma d_\sigma \bar{\chi}\chi)}_{\Lambda}$, for the three-legged boson–fermion vertices $\Gamma^{(\bar{d}_\uparrow d_\downarrow \chi)}_{\Lambda}$ and $\Gamma^{(\bar{d}_\downarrow d_\uparrow \bar{\chi})}_{\Lambda}$, as well as for the flowing irreducible spin-flip susceptibility $\Pi^{\perp}_{\Lambda}(\mathrm{i}\bar{\omega})$ which determines the single-scale spin-flip propagator $\dot{F}^{\perp}_{\Lambda}(\mathrm{i}\bar{\omega})$. The exact FRG flow equations for the three- and four-legged boson–fermion vertices have been written down diagrammatically in [20]; the crucial point is that the right-hand sides of these flow equations vanish at the initial scale $\Lambda = \Lambda_0$ because they depend on higher-order vertices which are not contained in the bare action. It is therefore reasonable to ignore the RG flow of the three- and four-legged boson–fermion vertices, which amounts to truncating the flow equation (3.6) by replacing these vertices by their initial values,

$$\Gamma^{(\bar{d}_\sigma d_\sigma \bar{\chi}\chi)}_{\Lambda}(\omega, \omega; \bar{\omega}, \bar{\omega}) \approx \Gamma^{(\bar{d}_\sigma d_\sigma \bar{\chi}\chi)}_{\Lambda_0}(\omega, \omega; \bar{\omega}, \bar{\omega}) = 0, \tag{3.10a}$$

$$\Gamma^{(\bar{d}_\uparrow d_\downarrow \chi)}_{\Lambda}(\omega, \omega-\bar{\omega}, \bar{\omega}) \approx \Gamma^{(\bar{d}_\uparrow d_\downarrow \chi)}_{\Lambda_0}(\omega, \omega-\bar{\omega}, \bar{\omega}) = 1, \tag{3.10b}$$

$$\Gamma^{(\bar{d}_\downarrow d_\uparrow \bar{\chi})}_{\Lambda}(\omega-\bar{\omega}, \omega, \bar{\omega}) \approx \Gamma^{(\bar{d}_\downarrow d_\uparrow \bar{\chi})}_{\Lambda_0}(\omega-\bar{\omega}, \omega, \bar{\omega}) = 1. \tag{3.10c}$$

To close our system of flow equations, we still need an additional equation for the flowing spin-flip susceptibility $\Pi^{\perp}_{\Lambda}(\mathrm{i}\bar{\omega})$, which in our cutoff scheme involves the pure boson vertex with four external legs [20]. Fortunately, we can avoid the explicit analysis of this equation by using the Dyson–Schwinger equation for our mixed boson–fermion theory, which implies an exact skeleton equation, relating the flowing spin-flip susceptibility to the flowing fermionic Green function $G^{\sigma}_{\Lambda}(\mathrm{i}\omega)$ and the flowing three-legged boson–fermion vertices. Using the same method as in appendix B of [17], we obtain the skeleton equation

$$\Pi^{\perp}_{\Lambda}(\mathrm{i}\bar{\omega}) = -\int_{\omega} G^{\uparrow}_{\Lambda}(\mathrm{i}\omega) G^{\downarrow}_{\Lambda}(\mathrm{i}\omega - \mathrm{i}\bar{\omega}) \Gamma^{(\bar{d}_\uparrow d_\downarrow \chi)}_{\Lambda}(\omega, \omega - \bar{\omega}, \bar{\omega})$$

$$= -\int_{\omega} G^{\uparrow}_{\Lambda}(\mathrm{i}\omega) G^{\downarrow}_{\Lambda}(\mathrm{i}\omega - \mathrm{i}\bar{\omega}) \Gamma^{(\bar{d}_\downarrow d_\uparrow \bar{\chi})}_{\Lambda}(\omega - \bar{\omega}, \omega, \bar{\omega}). \tag{3.11}$$

A graphical representation of this equation is shown in figure 6. Note that equation (3.7) guarantees that the two lines in equation (3.11) are indeed identical.

For simplicity, let us focus now on the non-magnetic case, where all correlation functions are spin independent and we may omit the spin labels. Given our approximation (3.10*b*) and (3.10*c*), the skeleton equation (3.11) then reduces to

$$\Pi^{\perp}_{\Lambda}(\mathrm{i}\bar{\omega}) = -\int_{\omega} G_{\Lambda}(\mathrm{i}\omega) G_{\Lambda}(\mathrm{i}\omega - \mathrm{i}\bar{\omega}), \tag{3.12}$$

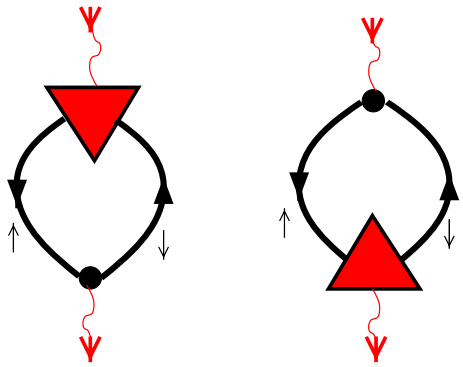

Figure 6. Graphical representation of the skeleton equation (3.11) relating the flowing spin-flip susceptibility $\Pi^{\perp}_{\Lambda}(\mathrm{i}\bar{\omega})$ to the exact fermionic Green functions and the three-legged boson–fermion vertices. The two diagrams are equivalent.

while the FRG flow equation (3.6) simplifies to

$$\partial_{\Lambda}\Sigma_{\Lambda}(\mathrm{i}\omega) = \int_{\bar{\omega}} \dot{F}^{\perp}_{\Lambda}(\mathrm{i}\bar{\omega}) G_{\Lambda}(\mathrm{i}\omega - \mathrm{i}\bar{\omega}). \tag{3.13}$$

Equations (3.12) and (3.13) form a closed system of integro-differential equations for the flowing self-energy $\Sigma_{\Lambda}(\mathrm{i}\omega)$ of the d electrons. Recall that equation (3.13) depends implicitly on the flowing spin-flip susceptibility via equations (3.4) and (3.5). Anticipating that there is no spontaneous magnetism, the initial condition (3.9) for the fermionic self-energy at scale $\Lambda = \Lambda_0$ is simply

$$\Sigma_{\Lambda_0}(\mathrm{i}\omega) = \frac{Un}{2}. \tag{3.14}$$

In the particle–hole symmetric case where $E_{\mathrm{d}} - \mu = -U/2$ and $n = 1$ this cancels precisely the energy $\xi^{\sigma}_0 = E_{\mathrm{d}} - \mu$ in the Hartree–Fock d electron propagator $G_{\Lambda_0}(\mathrm{i}\omega)$, which in the wide-band limit is therefore given by

$$G_{\Lambda_0}(\mathrm{i}\omega) = \frac{1}{\mathrm{i}\omega + \mathrm{i}\Delta\,\mathrm{sgn}\,\omega}. \tag{3.15}$$

We next show that the solution of equations (3.12) and (3.13) does not suffer from the Stoner instability and correctly predicts Fermi liquid behavior [1] for arbitrary U. We shall restrict ourselves to the particle–hole symmetric case from now on.

3.3. Low-energy truncation

The coupled system of integro-differential equations given by equations (3.4), (3.5), (3.12), (3.13) can be solved numerically for arbitrary frequencies, but this is beyond the scope of this work. Here, we shall focus on the low-frequency range $|\omega| \lesssim \Delta$. In this regime, it is reasonable to replace the flowing d electron propagator appearing on the right-hand sides of equations (3.12) and (3.13) by the low-frequency Fermi liquid form

$$G_{\Lambda}(\mathrm{i}\omega) = \frac{Z_l}{\mathrm{i}\omega + \mathrm{i}\Delta_l\,\mathrm{sgn}\,\omega}, \tag{3.16}$$

where the flowing wavefunction renormalization factor is defined by

$$Z_l = \frac{1}{1 - \frac{\partial \Sigma_\Lambda(\mathrm{i}\omega)}{\partial(\mathrm{i}\omega)}\Big|_{\omega=0}}, \tag{3.17}$$

and the renormalized flowing hybridization is

$$\Delta_l = Z_l \Delta. \tag{3.18}$$

We consider Z_l and Δ_l to be functions of the logarithmic flow parameter $l = -\ln(\Lambda/\Lambda_0)$. The approximation (3.16) is certainly not sufficient at high frequencies, so we cannot recover in this way the high-energy Hubbard peaks at strong coupling which are known to appear at an energy scale of order $U/2$.

Given the approximation (3.16), the frequency integration in equation (3.12) is easily carried out analytically, resulting in

$$\Pi^\perp_\Lambda(\mathrm{i}\bar\omega) = \frac{Z_l^2}{\pi|\bar\omega|}\frac{\ln\left(1+\frac{|\bar\omega|}{\Delta_l}\right)}{\left[1+\frac{|\bar\omega|}{2\Delta_l}\right]} = \frac{Z_l}{\pi\Delta} f\left(\frac{|\bar\omega|}{\Delta_l}\right), \tag{3.19}$$

with

$$f(x) = \frac{\ln(1+x)}{x(1+x/2)}. \tag{3.20}$$

Introducing the dimensionless coupling constants

$$u_l = Z_l u_0 = \frac{Z_l U}{\pi\Delta} = \frac{Z_l^2 U}{\pi\Delta_l}, \tag{3.21}$$

$$\lambda_l = \frac{\Lambda}{Z_l\Delta} = \frac{\Lambda}{\Delta_l}, \tag{3.22}$$

the single-scale propagator defined in (3.5) can then be written as

$$\dot F^\perp_\Lambda(\mathrm{i}\bar\omega) = -\frac{\pi}{Z_l^2}\frac{\Theta(\Lambda-|\bar\omega|)}{\left[\frac{1}{u_l}+\lambda_l-\frac{|\bar\omega|}{\Delta_l}-f(\frac{|\bar\omega|}{\Delta_l})\right]^2}. \tag{3.23}$$

Actually, for consistency with our approximation (3.16) which is based on the expansion of the fermionic self-energy to linear order in frequency, we should also expand the bosonic self-energy $\Pi^\perp_\Lambda(\mathrm{i}\bar\omega)$ to linear order in $\bar\omega$. Using $f(x) = 1 - x + \mathcal{O}(x^2)$, we have

$$\pi\Delta\Pi^\perp_\Lambda(\mathrm{i}\bar\omega) \approx Z_l - \frac{|\bar\omega|}{\Delta} + \mathcal{O}(\bar\omega^2). \tag{3.24}$$

As compared with the non-interacting susceptibility (2.20), the leading constant term in equation (3.24) is reduced by the wavefunction renormalization factor, while the linear term is not renormalized. In this approximation, our single-scale propagator (3.23) simplifies to

$$\dot F^\perp_\Lambda(\mathrm{i}\bar\omega) = -\frac{\pi}{Z_l^2}\frac{\Theta(\Lambda-|\bar\omega|)}{\left[\frac{1}{u_l}+\lambda_l-1\right]^2}, \tag{3.25}$$

which by construction of the regulator function given in equations (3.2) and (3.3) is constant for frequencies below the running cutoff Λ. To determine Z_l, we calculate the flowing anomalous dimension η_l, which is directly related to the derivative of the self-energy with respect to the flow parameter,

$$\eta_l = -\partial_l \ln Z_l = Z_l\Lambda \lim_{\omega\to0}\frac{\partial}{\partial(\mathrm{i}\omega)}\partial_\Lambda\Sigma_\Lambda(\mathrm{i}\omega). \tag{3.26}$$

Substituting equations (3.13) and (3.16), we obtain

$$\eta_l = Z_l^2\Lambda\lim_{\omega\to0}\frac{\partial}{\partial(\mathrm{i}\omega)}\int_{\bar\omega}\frac{\dot F^\perp_\Lambda(\mathrm{i}\bar\omega)}{\mathrm{i}\omega-\mathrm{i}\bar\omega+\mathrm{i}\Delta_l\,\mathrm{sgn}(\omega-\bar\omega)}. \tag{3.27}$$

If we naively interchange the order of integration and differentiation, we encounter an ambiguous expression of the form

$$\lim_{\omega\to0}\frac{\partial}{\partial(\mathrm{i}\omega)}\left[\frac{1}{\mathrm{i}\omega-\mathrm{i}\bar\omega+\mathrm{i}\Delta_l\,\mathrm{sgn}(\omega-\bar\omega)}\right] = \frac{1}{[\bar\omega+\Delta_l\,\mathrm{sgn}\,\bar\omega]^2} + \frac{2\Delta_l\delta(\bar\omega)}{[\Delta_l(2\Theta(\bar\omega)-1)]^2}, \tag{3.28}$$

where we have written $\mathrm{sgn}\,\bar\omega = 2\Theta(\bar\omega) - 1$. As pointed out by Morris [22], one should interpret the product of the delta function $\delta(x)$ with any function $f(\Theta(x))$ of the step function as

$$\delta(x) f(\Theta(x)) = \delta(x)\int_0^1 \mathrm{d}t f(t). \tag{3.29}$$

Using this relation, equation (3.28) reduces to

$$\lim_{\omega\to0}\frac{\partial}{\partial(\mathrm{i}\omega)}\left[\frac{1}{\mathrm{i}\omega-\mathrm{i}\bar\omega+\mathrm{i}\Delta_l\,\mathrm{sgn}(\omega-\bar\omega)}\right] = \frac{1}{[|\bar\omega|+\Delta_l]^2} - \frac{2\delta(\bar\omega)}{\Delta_l}, \tag{3.30}$$

so equation (3.27) takes the form

$$\eta_l = -\frac{Z_l\Lambda}{\pi\Delta}\dot F^\perp_\Lambda(\mathrm{i}0) + Z_l^2\Lambda\int_{\bar\omega}\frac{\dot F^\perp_\Lambda(\mathrm{i}\bar\omega)}{(|\bar\omega|+\Delta_l)^2}. \tag{3.31}$$

With the single-scale propagator given in equation (3.25), the frequency integration is trivial and we finally obtain from equation (3.27) for the flowing anomalous dimension

$$\eta_l = \frac{\lambda_l}{[1+\lambda_l][\frac{1}{u_l}+\lambda_l-1]^2}. \tag{3.32}$$

The right-hand side of this expression depends on Z_l via the flowing couplings u_l and λ_l defined in equations (3.21) and (3.22) such that

$$\partial_l Z_l = -\eta_l Z_l \tag{3.33}$$

is an ordinary differential equation for the flowing wavefunction renormalization factor Z_l, which is easily solved numerically. The result for the flowing Z_l is shown in figure 7. Obviously, for $l \to \infty$ the wavefunction renormalization factor approaches a finite limit, $Z = \lim_{l\to\infty} Z_l$, which we show in figure 8 as a function of the bare coupling u_0. We now obtain, in contrast to the ladder approximation result discussed in section 2, a finite Z for all values of the interaction, so the fluctuations included in our simple FRG approach are sufficient to remove the unphysical Stoner instability. On the other hand, quantitatively our truncation of the exact FRG flow equations does not reproduce the correct strong coupling behavior of the quasiparticle residue, which is known to exhibit the same

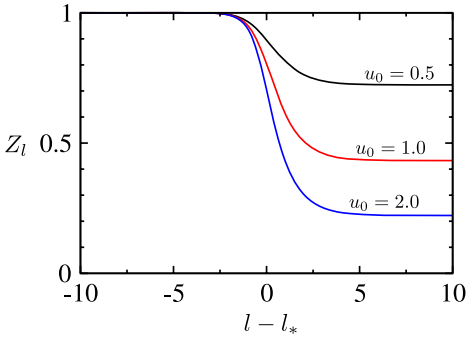

Figure 7. Numerical solution of equation (3.33) for different values of the bare coupling $u_0 = U/(\pi\Delta)$. Here, l_* is the scale where the running cutoff Λ is equal to the hybridization Δ, i.e., $\Lambda_0 e^{-l_*} = \Delta$.

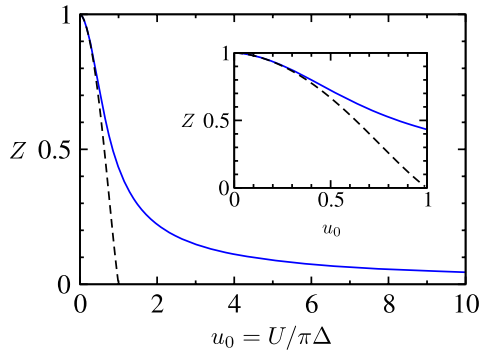

Figure 8. The solid line is the wavefunction renormalization factor $Z = \lim_{l\to\infty} Z_l$ as a function of the bare coupling u_0 obtained from the numerical solution of our truncated flow equation (3.33). For comparison, we show as the dashed line the result from the ladder approximation.

exponential suppression as the Kondo temperature for $u_0 \to \infty$ (see [23]),

$$Z_{\text{exact}} \sim \sqrt{\frac{8u_0}{\pi}}\exp[-\pi^2 u_0/8]. \tag{3.34}$$

From the numerical solution of our flow equation given in equations (3.32) and (3.33) we find asymptotically

$$Z \sim \frac{0.445}{u_0}, \qquad u_0 \gg 1. \tag{3.35}$$

The fact that this is much larger than the exact result (3.34) indicates that our approach underestimates the strength of fluctuations. In section 4 we shall therefore include the longitudinal spin fluctuation channel and show that it indeed further suppresses the value of Z, although within our approximations we are unable to recover the exponential suppression described by equation (3.34).

4. FRG with partial bosonization of transverse and longitudinal spin fluctuations

4.1. Multi-channel Hubbard–Stratonovich transformation

Using the antisymmetry of the Grassmann fields, the local Hubbard interaction can be written in infinitely many equivalent ways, such as

$$Un_\uparrow(\tau)n_\downarrow(\tau) = -\frac{U^\parallel}{2}m^2(\tau) - U^\perp \bar{s}(\tau)s(\tau), \tag{4.1}$$

where

$$U^\parallel + U^\perp = U. \tag{4.2}$$

Here, $n_\sigma(\tau) = \bar{d}_\sigma(\tau)d_\sigma(\tau)$ and the composite fields $m(\tau) = \sum_\sigma \sigma n_\sigma(\tau)$, $\bar{s}(\tau) = \bar{d}_\uparrow(\tau)d_\downarrow(\tau)$, and $s(\tau) = \bar{d}_\downarrow(\tau)d_\uparrow(\tau)$ represent the longitudinal and transverse spin components; see also equation (2.8). Note that by construction of the decomposition (4.1) we have included both longitudinal and transverse spin fluctuations, but no charge fluctuations. In section 3 we have satisfied equation (4.1) by setting $U^\parallel = 0$ and $U^\perp = U$, which is the natural choice if one is interested in bosonizing the transverse spin fluctuations. Alternatively, one could set $U^\parallel = U$ and $U^\perp = 0$, so longitudinal spin fluctuations can be introduced via a suitable Hubbard–Stratonovich field. The ambiguity associated with equations (4.1) and (4.2) has been discussed for many decades in the literature [24–29]. Depending on the physical problem of interest, certain special choices of $U^\parallel$ and $U^\perp$ can be advantageous [28]. At this point, we simply leave the precise values of $U^\parallel$ and $U^\perp$ unspecified but assume that both are positive and satisfy equation (4.2). Later we shall show that in the strong coupling regime of the particle–hole symmetric AIM the optimal choice is $U^\parallel = U/3$ and $U^\perp = 2U/3$. In this case the decomposition (4.1) is manifestly spin-rotational invariant and can be written as

$$Un_\uparrow(\tau)n_\downarrow(\tau) = -\frac{U}{6}(\vec{s}(\tau))^2, \tag{4.3}$$

where the composite vector field $\vec{s}(\tau) = d^\dagger(\tau)\vec{\sigma}d(\tau)$ represents the spin vector. Here, $d^\dagger(\tau) = [\bar{d}_\uparrow(\tau), \bar{d}_\downarrow(\tau)]$ and $\vec{\sigma}$ is the usual matrix vector of Pauli matrices.

Starting from the representation (4.1), we decouple the interaction in the longitudinal spin channel using a real Hubbard–Stratonovich field η and in the transverse spin channel using the complex Hubbard–Stratonovich fields χ and $\bar{\chi}$ introduced in section 2.2. The partition function can then be written as in equation (2.9), where $\Phi = [d_\uparrow, \bar{d}_\uparrow, d_\downarrow, \bar{d}_\downarrow, \eta, \chi, \bar{\chi}]$ is now a seven-component superfield. For the Gaussian part of the action we then obtain instead of equation (2.10)

$$S_0[\Phi] = -\int_\omega \sum_\sigma \left[G_0^\sigma(\mathrm{i}\omega)\right]^{-1}\bar{d}_{\omega\sigma}d_{\omega\sigma} + \int_{\bar{\omega}}(U^\perp)^{-1}\bar{\chi}_{\bar{\omega}}\chi_{\bar{\omega}} + \tfrac{1}{2}\int_{\bar{\omega}}(U^\parallel)^{-1}\eta_{-\bar{\omega}}\eta_{\bar{\omega}}, \tag{4.4}$$

and the interaction part can be written as

$$S_1[\Phi] = \int_{\bar{\omega}}\left[\bar{s}_{\bar{\omega}}\chi_{\bar{\omega}} + s_{\bar{\omega}}\bar{\chi}_{\bar{\omega}} + m_{-\bar{\omega}}\eta_{\bar{\omega}}\right] - \int_\omega \sum_\sigma \delta\xi^\sigma \bar{d}_{\omega\sigma}d_{\omega\sigma}. \tag{4.5}$$

The counterterm $\delta\xi^\sigma$ in equation (4.5) is subtracted to correct for the inclusion of the Hartree–Fock self-energy in the

propagator $G_0^\sigma(\mathrm{i}\omega)$ in equation (4.4). While the transverse spin components $s_{\bar\omega}$ and $\bar s_{\bar\omega}$ are given by equations (2.12) and (2.13), the longitudinal spin component is given by

$$m_{\bar\omega} = \int_0^\beta \mathrm{d}\tau \mathrm{e}^{\mathrm{i}\bar\omega\tau} m(\tau) = \int_\omega \sum_\sigma \sigma \bar d_{\omega\sigma}\, \mathrm{d}_{\omega+\bar\omega,\sigma}. \tag{4.6}$$

For simplicity, we shall focus here on the non-magnetic, particle–hole symmetric case. Since in the strong coupling limit the low-energy physics is expected to be dominated by spin fluctuations, we set up the FRG by introducing a cutoff only in the bosonic fields η, χ and $\bar\chi$ associated with spin fluctuations. Particle–hole symmetry guarantees that the exact self-energy at zero frequency cancels the term $E_\mathrm{d} - \mu$, so we may approximate $G_0^\sigma(\mathrm{i}\omega)$ by equation (3.15).

4.2. FRG flow equations

We now generalize equation (3.1) by introducing cutoffs into both kinds of bosonic propagators appearing in the Gaussian action (4.4),

$$(U^\alpha)^{-1} \to (U^\alpha)^{-1} + R_\Lambda^\alpha(\mathrm{i}\bar\omega), \tag{4.7}$$

where $\alpha = \parallel, \perp$ labels the two kinds of spin fluctuations, and the cutoff functions are

$$R^\parallel(\mathrm{i}\bar\omega) = \frac{2\Lambda}{\pi\Delta^2} R\left(\frac{|\bar\omega|}{\Lambda}\right), \tag{4.8a}$$

$$R^\perp(\mathrm{i}\bar\omega) = \frac{\Lambda}{\pi\Delta^2} R\left(\frac{|\bar\omega|}{\Lambda}\right), \tag{4.8b}$$

with $R(x)$ given in equation (3.3). From the general FRG flow equations for mixed boson–fermion theories given in [17, 19] we then obtain the following exact flow equation for the self-energy,

$$\begin{aligned}
\partial_\Lambda \Sigma_\Lambda^\sigma(\mathrm{i}\omega) = {} & \int_{\bar\omega} \dot F_\Lambda^\parallel(\mathrm{i}\bar\omega)\Gamma_\Lambda^{(\bar d_\sigma d_\sigma \eta\eta)}(\omega,\omega;\bar\omega,-\bar\omega) \\
& + \int_{\bar\omega} \dot F_\Lambda^\perp(\mathrm{i}\bar\omega)\Gamma_\Lambda^{(\bar d_\sigma d_\sigma \bar\chi\chi)}(\omega,\omega;\bar\omega,\bar\omega) \\
& + \int_{\bar\omega} \dot F_\Lambda^\parallel(\mathrm{i}\bar\omega) G_\Lambda^\sigma(\mathrm{i}\omega - \mathrm{i}\bar\omega)\Gamma_\Lambda^{(\bar d_\sigma d_\sigma \eta)}(\omega,\omega-\bar\omega,\bar\omega) \\
& \times \Gamma_\Lambda^{(\bar d_\sigma d_\sigma \eta)}(\omega-\bar\omega,\omega,-\bar\omega) \\
& + \int_{\bar\omega} \dot F_\Lambda^\perp(\mathrm{i}\bar\omega) G_\Lambda^{\bar\sigma}(\mathrm{i}\omega - \mathrm{i}\sigma\bar\omega)\Gamma_\Lambda^{(\bar d_\sigma d_{\bar\sigma}\chi_\sigma)}(\omega,\omega-\sigma\bar\omega,\sigma\bar\omega) \\
& \times \Gamma_\Lambda^{(\bar d_{\bar\sigma} d_\sigma \chi_{\bar\sigma})}(\omega-\sigma\bar\omega,\omega,\sigma\bar\omega),
\end{aligned} \tag{4.9}$$

which generalizes equation (3.6) and is shown graphically in figure 9. The superscripts label the different kinds of vertices; for the boson–fermion vertices associated with the transverse spin field we have used again the short notation $\chi_\uparrow = \chi$ and $\chi_\downarrow = \bar\chi$; see equation (3.6). The longitudinal and transverse single-scale propagators are

$$\dot F_\Lambda^\alpha(\mathrm{i}\bar\omega) = [-\partial_\Lambda R_\Lambda^\alpha(\mathrm{i}\bar\omega)][F_\Lambda^\alpha(\mathrm{i}\bar\omega)]^2, \tag{4.10}$$

with

$$F_\Lambda^\alpha(\mathrm{i}\bar\omega) = [(U^\alpha)^{-1} - \Pi_\Lambda^\alpha(\mathrm{i}\bar\omega) + R_\Lambda^\alpha(\mathrm{i}\bar\omega)]^{-1}, \tag{4.11}$$

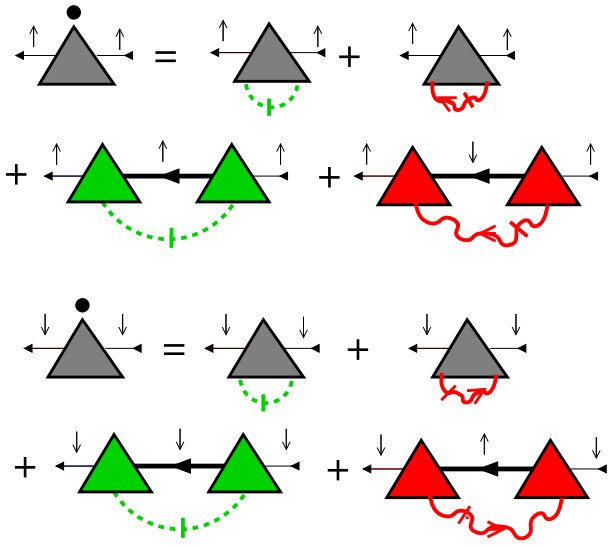

Figure 9. Graphical representation of the exact FRG flow equation (4.9) for the self-energies $\Sigma_\Lambda^\uparrow$ and $\Sigma_\Lambda^\downarrow$. The longitudinal spin field η is represented by dashed lines; the other symbols are the same as in figure 5.

where $\Pi_\Lambda^\alpha(\mathrm{i}\bar\omega)$ are the corresponding irreducible spin susceptibilities. As discussed in section 3.2, we use the skeleton equations (which can be formally derived from the Dyson–Schwinger equations) to relate the flow of the susceptibilities to the flow of the d electron propagators and the three-legged boson–fermion vertex. The skeleton equation for the transverse susceptibility $\Pi_\Lambda^\perp(\mathrm{i}\bar\omega)$ has already been discussed in section 3.2, see equation (3.11); it can also be written as

$$\begin{aligned}
\Pi_\Lambda^\perp(\mathrm{i}\bar\omega) = {} & -\int_\omega G_\Lambda^\sigma(\mathrm{i}\omega) G_\Lambda^{\bar\sigma}(\mathrm{i}\omega - \mathrm{i}\sigma\bar\omega) \\
& \times \Gamma_\Lambda^{(\bar d_\sigma d_{\bar\sigma}\chi_\sigma)}(\omega,\omega-\sigma\bar\omega,\bar\omega).
\end{aligned} \tag{4.12}$$

The corresponding skeleton equation for the longitudinal spin susceptibility is

$$\begin{aligned}
\Pi_\Lambda^\parallel(\mathrm{i}\bar\omega) = {} & -\int_\omega \sum_\sigma \sigma G_\Lambda^\sigma(\mathrm{i}\omega) G_\Lambda^\sigma(\mathrm{i}\omega - \mathrm{i}\bar\omega) \\
& \times \Gamma_\Lambda^{(\bar d_\sigma d_\sigma \eta)}(\omega,\omega-\bar\omega,\bar\omega).
\end{aligned} \tag{4.13}$$

To obtain a closed RG flow equation for the self-energy, we still need flow equations for the vertices with three and four external legs appearing in equation (4.9). As in section 3.2, we simply set all mixed boson–fermion vertices with four external legs equal to zero, because these vertices vanish at the initial scale. However, in contrast to the case for the FRG with only transverse spin fluctuations discussed in section 3.2, the renormalization of the three-legged boson–fermion vertices is now important. In the approximation where mixed boson–fermion vertices with four and more external legs are ignored, the FRG flow equation for the longitudinal three-legged boson–fermion vertex is

$$\begin{aligned}
& \partial_\Lambda \Gamma_\Lambda^{(\bar d_\sigma d_\sigma \eta)}(\omega+\bar\omega,\omega,\bar\omega) \\
& \quad = \int_{\bar\omega'} \dot F_\Lambda^\parallel(\mathrm{i}\bar\omega') G_\Lambda^\sigma(\mathrm{i}\omega + \mathrm{i}\bar\omega + i\bar\omega') G_\Lambda^\sigma(\mathrm{i}\omega + \mathrm{i}\bar\omega')
\end{aligned}$$

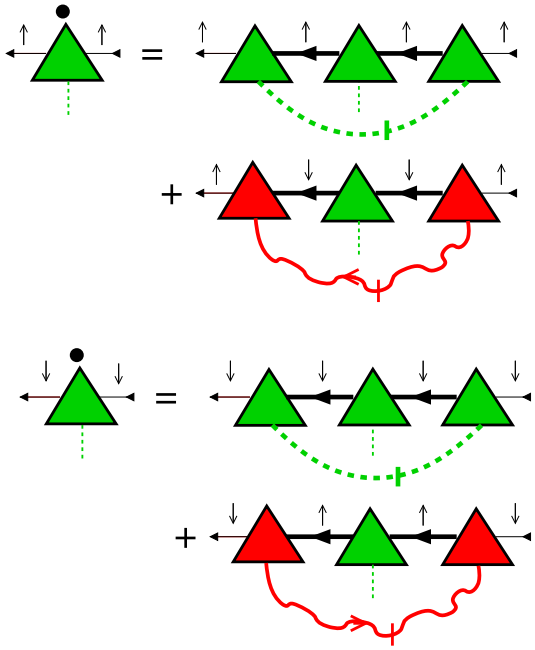

Figure 10. Graphical representation of the FRG flow equation (4.14) for the longitudinal boson–fermion vertices $\Gamma_\Lambda^{(\bar{d}_\uparrow d_\uparrow \eta)}$ (upper graph) and $\Gamma_\Lambda^{(\bar{d}_\downarrow d_\downarrow \eta)}$ (lower graph).

$$
\begin{aligned}
&\times \Gamma_\Lambda^{(\bar{d}_\sigma d_\sigma \eta)}(\omega+\bar{\omega},\omega+\bar{\omega}+\bar{\omega}',-\bar{\omega}')\\
&\times \Gamma_\Lambda^{(\bar{d}_\sigma d_\sigma \eta)}(\omega+\bar{\omega}+\bar{\omega}',\omega+\bar{\omega}',\bar{\omega})\\
&\times \Gamma_\Lambda^{(\bar{d}_\sigma d_\sigma \eta)}(\omega+\bar{\omega}',\omega,\bar{\omega}')\\
&+\int_{\bar{\omega}'} \dot{F}_\Lambda^{\perp}(-\mathrm{i}\sigma\bar{\omega}')G_\Lambda^{\bar{\sigma}}(\mathrm{i}\omega+\mathrm{i}\bar{\omega}+\mathrm{i}\bar{\omega}')G_\Lambda^{\bar{\sigma}}(\mathrm{i}\omega+\mathrm{i}\bar{\omega}')\\
&\times \Gamma_\Lambda^{(\bar{d}_\sigma d_{\bar{\sigma}} \chi_\sigma)}(\omega+\bar{\omega},\omega+\bar{\omega}+\bar{\omega}',-\sigma\bar{\omega}')\\
&\times \Gamma_\Lambda^{(\bar{d}_\sigma d_\sigma \eta)}(\omega+\bar{\omega}+\bar{\omega}',\omega+\bar{\omega}',\bar{\omega})\\
&\times \Gamma_\Lambda^{(\bar{d}_{\bar{\sigma}} d_\sigma \chi_{\bar{\sigma}})}(\omega+\bar{\omega}',\omega,-\sigma\bar{\omega}'),
\end{aligned}
\tag{4.14}
$$

while the corresponding flow equation for the transverse vertex reads

$$
\begin{aligned}
&\partial_\Lambda \Gamma_\Lambda^{(\bar{d}_\sigma d_{\bar{\sigma}} \chi_\sigma)}(\omega+\bar{\omega},\omega,\sigma\bar{\omega})\\
&\quad=\int_{\bar{\omega}'} \dot{F}_\Lambda^{\parallel}(\mathrm{i}\bar{\omega}')G_\Lambda^{\sigma}(\mathrm{i}\omega+\mathrm{i}\bar{\omega}+\mathrm{i}\bar{\omega}')G_\Lambda^{\bar{\sigma}}(\mathrm{i}\omega+\mathrm{i}\bar{\omega}')\\
&\qquad\times \Gamma_\Lambda^{(\bar{d}_\sigma d_\sigma \eta)}(\omega+\bar{\omega},\omega+\bar{\omega}+\bar{\omega}',-\bar{\omega}')\\
&\qquad\times \Gamma_\Lambda^{(\bar{d}_\sigma d_{\bar{\sigma}} \chi_\sigma)}(\omega+\bar{\omega}+\bar{\omega}',\omega+\bar{\omega}',\sigma\bar{\omega})\\
&\qquad\times \Gamma_\Lambda^{(\bar{d}_{\bar{\sigma}} d_\sigma \eta)}(\omega+\bar{\omega}',\omega,\bar{\omega}').
\end{aligned}
\tag{4.15}
$$

Graphical representations of equations (4.14) and (4.15) are shown in figures 10 and 11. From $S_1[\Phi]$ in equation (4.5) we see that the initial conditions for the three-legged vertices at scale $\Lambda=\Lambda_0$ are

$$\Gamma_{\Lambda_0}^{(\bar{d}_\sigma d_\sigma \eta)}(\omega+\bar{\omega},\omega,\bar{\omega})=\sigma, \tag{4.16a}$$

$$\Gamma_{\Lambda_0}^{(\bar{d}_\sigma d_{\bar{\sigma}} \chi_\sigma)}(\omega+\bar{\omega},\omega,\sigma\bar{\omega})=1. \tag{4.16b}$$

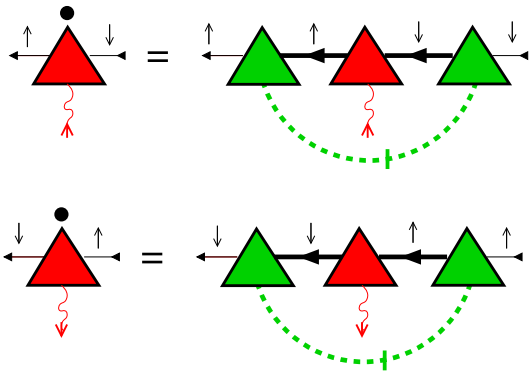

Figure 11. Graphical representation of the FRG flow equation (4.15) for the transverse boson–fermion vertices $\Gamma_\Lambda^{(\bar{d}_\uparrow d_\downarrow \chi)}$ (upper graph) and $\Gamma_\Lambda^{(\bar{d}_\downarrow d_\uparrow \bar{\chi})}$ (lower graph).

4.3. Low-energy truncation

To make further progress, we now neglect the frequency dependence of the three-legged boson–fermion vertices, setting

$$\Gamma_\Lambda^{(\bar{d}_\sigma d_\sigma \eta)}(\omega+\bar{\omega},\omega,\bar{\omega})\approx\sigma\gamma_\Lambda^{\parallel}, \tag{4.17}$$

$$\Gamma_\Lambda^{(\bar{d}_\sigma d_{\bar{\sigma}} \chi_\sigma)}(\omega+\bar{\omega},\omega,\sigma\bar{\omega})\approx\gamma_\Lambda^{\perp}. \tag{4.18}$$

Keeping in mind that we have also neglected all vertices involving more than three external legs, our exact FRG flow equation (4.9) for the self-energy reduces to

$$
\begin{aligned}
\partial_\Lambda \Sigma_\Lambda^{\sigma}(\mathrm{i}\omega)&=(\gamma_\Lambda^{\parallel})^2\int_{\bar{\omega}} \dot{F}_\Lambda^{\parallel}(\mathrm{i}\bar{\omega})G_\Lambda^{\sigma}(\mathrm{i}\omega-\mathrm{i}\bar{\omega})\\
&\quad+(\gamma_\Lambda^{\perp})^2\int_{\bar{\omega}} \dot{F}_\Lambda^{\perp}(\mathrm{i}\bar{\omega})G_\Lambda^{\bar{\sigma}}(\mathrm{i}\omega-\mathrm{i}\sigma\bar{\omega}).
\end{aligned}
\tag{4.19}
$$

Moreover, the approximate FRG flow equation (4.14) for the longitudinal spin-fermion vertex reduces to

$$
\begin{aligned}
\partial_\Lambda \gamma_\Lambda^{\parallel}&=(\gamma_\Lambda^{\parallel})^3\int_{\bar{\omega}} \dot{F}_\Lambda^{\parallel}(\mathrm{i}\bar{\omega})[G_\Lambda^{\uparrow}(\mathrm{i}\bar{\omega})]^2\\
&\quad-\gamma_\Lambda^{\parallel}(\gamma_\Lambda^{\perp})^2\int_{\bar{\omega}} \dot{F}_\Lambda^{\perp}(\mathrm{i}\bar{\omega})[G_\Lambda^{\downarrow}(-\mathrm{i}\bar{\omega})]^2,
\end{aligned}
\tag{4.20}
$$

while the FRG equation (4.15) for the transverse spin-fermion vertex becomes

$$\partial_\Lambda \gamma_\Lambda^{\perp}=-\gamma_\Lambda^{\perp}(\gamma_\Lambda^{\parallel})^2\int_{\bar{\omega}} \dot{F}_\Lambda^{\parallel}(\mathrm{i}\bar{\omega})G_\Lambda^{\uparrow}(\mathrm{i}\bar{\omega})G_\Lambda^{\downarrow}(\mathrm{i}\bar{\omega}). \tag{4.21}$$

Within the same approximation, the skeleton equations (4.12) and (4.13) for the spin susceptibilities are

$$\Pi_\Lambda^{\parallel}(\mathrm{i}\bar{\omega})=-\gamma_\Lambda^{\parallel}\int_\omega\sum_\sigma G_\Lambda^{\sigma}(\mathrm{i}\omega)G_\Lambda^{\sigma}(\mathrm{i}\omega-\mathrm{i}\bar{\omega}), \tag{4.22}$$

$$\Pi_\Lambda^{\perp}(\mathrm{i}\bar{\omega})=-\gamma_\Lambda^{\perp}\int_\omega G_\Lambda^{\sigma}(\mathrm{i}\omega)G_\Lambda^{\bar{\sigma}}(\mathrm{i}\omega-\mathrm{i}\sigma\bar{\omega}). \tag{4.23}$$

Equations (4.19)–(4.23) form a closed system of integro-differential equations for the frequency-dependent self-energy $\Sigma_\Lambda^{\sigma}(\mathrm{i}\omega)$ and the frequency-independent parts $\gamma_\Lambda^{\parallel}$ and $\gamma_\Lambda^{\perp}$ of the three-legged boson–fermion vertices. In order to make

progress analytically, let us now approximate the flowing d electron Green function on the right-hand sides of the flow equation by its low-energy Fermi liquid form (3.16). Then the integrations in equations (4.22) and (4.23) can be performed analytically. For simplicity, we focus again on the non-magnetic particle–hole symmetric case and omit the spin labels. We then obtain

$$\Pi_\Lambda^\parallel(\mathrm{i}\bar\omega) = \frac{2Z_l}{\pi\Delta}\gamma_l^\parallel f\left(\frac{|\bar\omega|}{\Delta_l}\right), \tag{4.24}$$

$$\Pi_\Lambda^\perp(\mathrm{i}\bar\omega) = \frac{Z_l}{\pi\Delta}\gamma_l^\perp f\left(\frac{|\bar\omega|}{\Delta_l}\right), \tag{4.25}$$

where the function $f(x)$ is given in equation (3.20). The bosonic single-scale propagators can then be written as

$$\dot F_\Lambda^\parallel(\mathrm{i}\bar\omega) = -\frac{\pi}{2Z_l^2}\frac{\Theta(\Lambda-|\bar\omega|)}{\left[\frac{1}{u_l^\parallel}+\lambda_l-\frac{|\bar\omega|}{\Delta_l}-\gamma_l^\parallel f\left(\frac{|\bar\omega|}{\Delta_l}\right)\right]^2}, \tag{4.26}$$

$$\dot F_\Lambda^\perp(\mathrm{i}\bar\omega) = -\frac{\pi}{Z_l^2}\frac{\Theta(\Lambda-|\bar\omega|)}{\left[\frac{1}{u_l^\perp}+\lambda_l-\frac{|\bar\omega|}{\Delta_l}-\gamma_l^\perp f\left(\frac{|\bar\omega|}{\Delta_l}\right)\right]^2}. \tag{4.27}$$

Here, we have introduced again the notation $\lambda_l = \Lambda/\Delta_l = \Lambda/(Z_l\Delta)$, and the running interaction constants $u_l^\parallel$ and $u_l^\perp$ are defined by

$$u_l^\parallel = Z_l\frac{2U^\parallel}{\pi\Delta}, \qquad u_l^\perp = Z_l\frac{U^\perp}{\pi\Delta}. \tag{4.28}$$

In terms of the dimensionless bare couplings $u_0^\parallel$ and $u_0^\perp$ the condition (4.2) reads

$$u_0^\parallel/2 + u_0^\perp = u_0. \tag{4.29}$$

As discussed in section 3.3, for consistency we expand the function $f(|\bar\omega|/\Delta_l)$ in equations (4.24) and (4.25) to linear order in frequency as in equation (3.24). Then the frequency integrations in equations (4.19)–(4.21) can be performed analytically and we obtain the following system of RG flow equations for the three running couplings Z_l, $\gamma_l^\parallel$, and $\gamma_l^\perp$,

$$\frac{\partial_l Z_l}{Z_l} = -\eta_l^\parallel - \eta_l^\perp, \tag{4.30}$$

$$\frac{\partial_l \gamma_l^\parallel}{\gamma_l^\parallel} = -\frac{1}{2}A_l^\parallel + A_l^\perp, \tag{4.31}$$

$$\frac{\partial_l \gamma_l^\perp}{\gamma_l^\perp} = \frac{1}{2}A_l^\parallel, \tag{4.32}$$

where

$$\eta_l^\parallel = \frac{(\gamma_l^\parallel)^2\lambda_l}{2[1/u_l^\parallel+\lambda_l-\gamma_l^\parallel]^2} - \frac{1}{2}A_l^\parallel, \tag{4.33}$$

$$\eta_l^\perp = \frac{(\gamma_l^\perp)^2\lambda_l}{[1/u_l^\perp+\lambda_l-\gamma_l^\perp]^2} - A_l^\perp, \tag{4.34}$$

$$A_l^\alpha = (\gamma_l^\alpha)^2\lambda_l I(1/u_l^\alpha+\lambda_l-\gamma_l^\alpha, \gamma_l^\alpha-1, \lambda_l). \tag{4.35}$$

Here, we have introduced the dimensionless integral

$$\begin{aligned} I(a,b,\lambda) &= \int_0^\lambda \mathrm{d}x \frac{1}{(a+bx)^2(1+x)^2} \\ &= \frac{\lambda}{(a-b)^2}\left[\frac{1}{1+\lambda}+\frac{b^2}{a(a+b\lambda)}\right] \\ &\quad - \frac{2b}{(a-b)^3}\ln\left[\frac{a(1+\lambda)}{a+b\lambda}\right]. \end{aligned} \tag{4.36}$$

Of special interest is the manifestly spin-rotationally invariant decomposition (4.3). In this case $U^\parallel = U^\perp/2 = U/3$, such that each of the longitudinal and two transverse channels has the same weight. In terms of the dimensionless bare couplings $u_0^\parallel$ and $u_0^\perp$ defined in equations (4.28) we therefore have $u_0^\parallel = u_0^\perp = 2u_0/3$. It is now easy to see that for any l we have $u_l^\parallel = u_l^\perp = 2u_l/3$ with $u_l = Z_l u_0$ and $\gamma_l \equiv \gamma_l^\parallel = \gamma_l^\perp$. Our flow equations (4.30)–(4.32) then reduce to

$$\frac{\partial_l Z_l}{Z_l} = -\eta_l, \tag{4.37}$$

$$\frac{\partial_l \gamma_l}{\gamma_l} = \frac{1}{2}A_l, \tag{4.38}$$

where

$$\eta_l = \frac{3\gamma_l^2\lambda_l}{2\left[3/(2u_l)+\lambda_l-\gamma_l\right]^2} - \frac{3}{2}A_l, \tag{4.39}$$

$$A_l = \gamma_l^2\lambda_l I\left(3/(2u_l)+\lambda_l-\gamma_l, \gamma_l-1, \lambda_l\right). \tag{4.40}$$

The factors of 3 appearing here are related to the fact that for this choice of parameters we have three equivalent channels. Clearly, our truncated flow equations respect the spin-rotation symmetry of the problem such that for this special decomposition we can expect the best results.

4.4. Results

The three-dimensional system of differential equations given in equations (4.30)–(4.32) can easily be solved numerically. An example of a typical RG flow is shown in figure 12. Obviously, the wavefunction renormalization factor decreases monotonically as the RG is iterated, while the vertex corrections $\gamma_l^\parallel$ and $\gamma_l^\perp$ both increase. The strongest variations occur at the scale l_* where the effective cutoff $\Lambda_0 \mathrm{e}^{-l_*}$ is equal to the hybridization Δ.

Before discussing the behavior of $Z = \lim_{l\to\infty} Z_l$ in the strong coupling regime, let us fix the optimal choice of the relative weight of the bare couplings $U^\parallel$ and $U^\perp$ in the Hubbard–Stratonovich decoupling (4.1). In figure 13 we show the dependence of the wavefunction renormalization factor on the choice of $u_0^\parallel/u_0^\perp$ for fixed values of u_0. It turns out that all curves have a pronounced plateau with a minimum precisely at $u_0^\parallel/u_0^\perp = 1$, which corresponds to the manifestly spin-rotationally invariant decoupling (4.3). If we fix the choice of the Hubbard–Stratonovich decoupling by demanding that first-order variations of the results around the optimal choice should vanish, then we are naturally led to the decoupling (4.3). For the rest of this section we shall therefore use the manifestly spin-rotationally invariant choice $u_0^\parallel = u_0^\perp = 2u_0/3$.

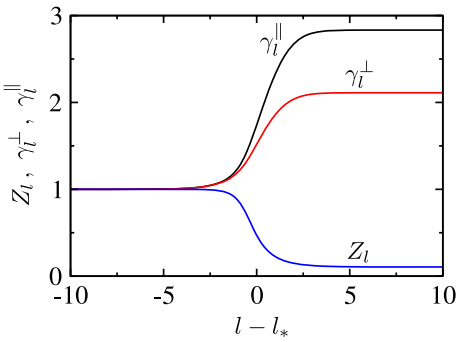

Figure 12. Typical flow of the wavefunction renormalization factor Z_l and of the frequency-independent parts $\gamma_l^{\perp}$ and $\gamma_l^{\parallel}$ of the boson–fermion vertices obtained from the numerical solution of equations (4.30)–(4.32). The scale $l_* = \ln(\Lambda_0/\Delta)$ is the same as in figure 7. The curves are for $u_0^{\parallel} = 1$ and $u_0^{\perp} = 1.5$, such that $u_0 = u_0^{\parallel}/2 + u_0^{\perp} = 2$.

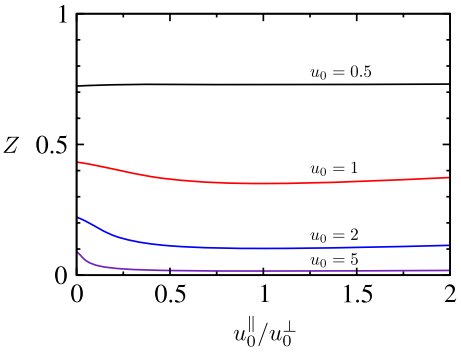

Figure 13. Dependence of the quasiparticle residue Z on the choice of the Hubbard–Stratonovich decoupling, parameterized by the ratio $u_0^{\parallel}/u_0^{\perp}$, with $u_0^{\parallel}/2 + u_0^{\perp} = u_0$. All curves exhibit a local minimum precisely at $u_0^{\parallel}/u_0^{\perp} = 1$, corresponding to the manifestly spin-rotationally invariant decoupling $u_0^{\parallel} = u_0^{\perp} = 2u_0/3$. While this minimum is also the global minimum for $u_0 = 1$, 2 and 5, it is only a local minimum for $u_0 = 0.5$. In fact, for $u_0 = 0.5$ the curve is almost flat and has a global minimum at $u_0^{\parallel}/u_0^{\perp} = 0$ and a local maximum between the two minima.

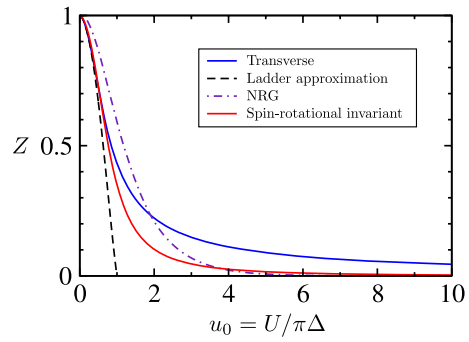

Figure 14. Wavefunction renormalization factor $Z = \lim_{l\to\infty} Z_l$ as a function of the bare coupling $u_0 = U/(\pi\Delta)$ obtained from the numerical solution of equations (4.30)–(4.32). The two-channel FRG results are for the manifestly spin-rotationally invariant choice of the two Hubbard–Stratonovich decouplings where $u_0^{\parallel} = u_0^{\perp} = 2u_0/3$. For comparison, we have also shown NRG results from [16] (which we have extrapolated to values $u_0 \gtrsim 4.5$).

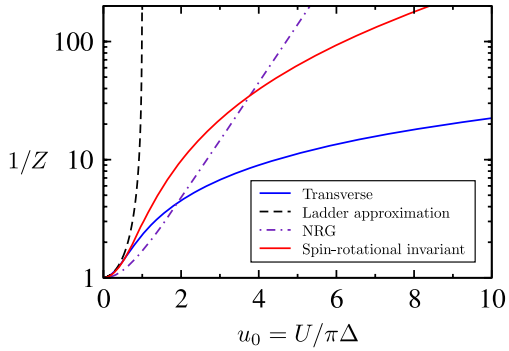

Figure 15. Redrawing of figure 14: the inverse wavefunction renormalization factor $1/Z$ is now plotted on a logarithmic scale.

In figure 14 we show our numerical results for Z as a function of the dimensionless bare coupling u_0. For comparison, we also show the prediction of the ladder approximation, as well as our FRG results with decoupling only in the transverse spin channel, and numerically accurate results obtained within Wilson's numerical renormalization group [16]. Our FRG calculation with simultaneous decoupling in both transverse and longitudinal spin channels obviously yields much better results for the suppression of Z in the strong coupling regime than the single-channel FRG discussed in section 3. In fact, on the scale of figure 14 our FRG results for Z seem to be reasonably close to the exact numerical results, which in the strong coupling regime can be approximated by the asymptotic formula (3.34). To investigate whether our FRG approach reproduces the known exponential suppression of Z, it is useful to present the data in figure 14 by plotting $1/Z$ on a logarithmic scale, as shown in figure 15. Note that on this scale the exponential suppression of Z at strong coupling corresponds to a straight line. Obviously, for $U \gtrsim 15\Delta$ our two-channel FRG results begin to deviate significantly from the NRG results and definitely do not reproduce the known exponential suppression of the quasiparticle weight for $U \to \infty$. On the other hand, the two-channel FRG is accurate up to $U \approx 15\Delta$. We suspect that the deviations from the NRG results for $U \lesssim 15\Delta$ are due to our linearization of the spin susceptibility, which is expected to lead to a suppression of the quasiparticle weight; see figure 4.

Finally, we show in figure 16 the spectral density of the d electrons, which is defined by

$$A(\omega) = -\frac{1}{\pi}\,\mathrm{Im}\,G(\omega + \mathrm{i}0). \tag{4.41}$$

For simplicity, we approximate $G(\omega + \mathrm{i}0)$ by $G_{\Lambda=0}(\mathrm{i}\omega \to \omega + \mathrm{i}0)$ and obtain

$$\pi\Delta A(\omega) = \frac{1}{1 + \left(\frac{\omega}{Z\Delta}\right)^2}, \tag{4.42}$$

with $Z = \lim_{l\to\infty} Z_l$. The qualitative behavior of $A(\omega)$ is in agreement with known results [1]: the width of the central Kondo peak is proportional to the wavefunction renormalization factor Z and its height at zero frequency is

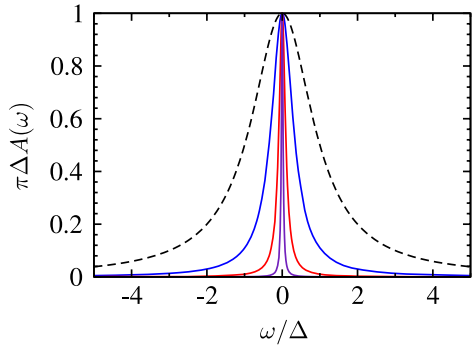

Figure 16. Low-energy behavior of the spectral density $A(\omega)$ of the d electrons as defined in equation (4.42) for $u_0 = 0$ (dashed line) and 1, 2, 4.

pinned to the value $1/(\pi\Delta)$ in the particle–hole symmetric case considered here, so the overall spectral weight of the low-energy peak is of order Z. In fact, the pinning of the central Kondo peak to the value $1/(\pi\Delta)$ is a simple consequence of the low-frequency Fermi liquid form of the flowing d electron propagator (3.16). The spectral line-shape at energies larger than Δ (including the broadened Hubbard bands at energy scales $\pm U/2$) cannot be described within our low-energy truncation.

5. Summary and conclusions

In summary, we have proposed a functional renormalization group approach to the Anderson impurity model which is based on the mapping of the original fermionic problem onto a mixed Bose–Fermi theory where the spin fluctuations are represented by bosonic Hubbard–Stratonovich fields. Our approach can be used to approximately calculate the spectral properties including the quasiparticle weight up to couplings $U \lesssim 15\Delta$.

This work also contains several technical advances which will be useful for other FRG calculations. In particular, we have shown that in FRG calculations for Fermi systems using the technique of partial bosonization [17–19, 30–32], the skeleton equations in the bosonic sector (which follow from the Dyson–Schwinger equations) can be used to close the FRG flow equations in the fermionic sector. Moreover, we have shown how the ambiguities inherent in multi-field Hubbard–Stratonovich decouplings can be resolved if one demands minimal sensitivity with respect to small variations of a given choice of decoupling. For a symmetric Anderson impurity model, this naturally leads to the manifestly spin-rotationally symmetric decoupling (4.3) at strong coupling. With our decoupling scheme, this symmetry is also respected by the truncated flow equations.

We have not been able to reproduce the exponential dependence $Z \propto \exp[-\pi^2 u_0/8]$ of the wavefunction renormalization factor for $U \to \infty$. Although we have tried several modifications of our approach, the strong fluctuations responsible for an exponential suppression of Z for $U \to \infty$ are apparently not correctly described within our truncation of the exact FRG flow equations. In order to make progress without using more elaborate numerical methods, we have made approximations which are only accurate at low energies $|\omega| \lesssim \Delta$. The first approximation is the linearization of the polarization in the bosonic propagator (4.11). In addition, we have also neglected the energy dependence of the three-legged boson–fermion interaction. Another approximation is the neglect of the four-legged boson–fermion vertex in our RG scheme. This was done (i) because this vertex vanishes in our initial mixed Bose–Fermi model and (ii) because it can be shown by means of a power counting analysis that this vertex is irrelevant in the RG sense and, therefore, becomes less important in the low-energy limit. In fact, all approximations made can be justified by means of a power counting analysis, showing that the neglected contributions are irrelevant in the RG sense. However, although it seems reasonable to neglect these kinds of contributions in a first approximation as is done here, these irrelevant couplings do have an effect, especially at strong coupling.

Finally, we point out that a direct numerical solution of our FRG flow equations should give rise to a better agreement with NRG data at small couplings U. Therefore one should numerically solve the coupled system of integro-differential equations given by equations (3.12) and (3.13) or equations (4.19)–(4.23), without approximating the fermionic Green function on the right-hand side of these equations by the Fermi liquid form (3.16). The fact that with our simple approximations we get results which agree reasonably well with NRG results gives us hope that solving this coupled system of integro-differential equations could lead to better results. Another direction of research which also deserves further investigation consists of analyzing how different truncation schemes of our exact Bose–Fermi hierarchy of RG flow equations would affect our results. This study would be clearly important in order to further improve our results for the dependence on U of the Kondo scale which is an intrinsic property of the Anderson impurity model.

Acknowledgments

We would like to acknowledge useful conversations with W Hofstetter, T Pruschke and A Sinner. Part of the work by PK was performed during a visit at the International Center for Condensed Matter Physics at the University of Brasília which was financially supported by the DAAD/PROBRAL program. JJRC gratefully acknowledges a DAAD postdoc fellowship.

References

[1] Hewson A C 1993 *The Kondo Problem to Heavy Fermions* (Cambridge: Cambridge University Press)
[2] Anderson P W 1961 *Phys. Rev.* B **124** 41
Anderson P W 1978 *Rev. Mod. Phys.* **50** 191
[3] Wilson K G 1975 *Rev. Mod. Phys.* **47** 773
[4] Costi T A, Hewson A C and Zlatić V 1994 *J. Phys.: Condens. Matter* **6** 2519
[5] Hofstetter W 2000 *Phys. Rev. Lett.* **85** 1508
[6] Bulla R, Costi T A and Pruschke T 2008 *Rev. Mod. Phys.* **80** 395
[7] Georges A, Kotliar G, Krauth W and Rozenberg M J 1996 *Rev. Mod. Phys.* **68** 13

[8] Newns D M and Read J 1983 *J. Phys. C: Solid State Phys.* **16** 3273
Newns D M and Read J 1988 *Adv. Phys.* **36** 799
[9] Coleman P 1984 *Phys. Rev.* B **29** 3035
[10] Mueller-Hartmann E 1984 *Z. Phys.* B **57** 281
[11] Logan D E, Eastwood M P and Tusch M A 1998 *J. Phys.: Condens. Matter* **10** 2673
Dickens N L and Logan D 2001 *J. Phys.: Condens. Matter* **13** 4505
[12] Hewson A C 2001 *J. Phys.: Condens. Matter* **13** 10011
[13] Kroha J and Wölfle P 2004 *Theoretical Methods for Strongly Correlated Electrons* ed D Sénéchal, A-M Tremblay and C Bourbonnais (Berlin: Springer)
[14] Janiš V and Augustinskỳ P 2007 *Phys. Rev.* B **75** 165108
Janiš V and Augustinskỳ P 2008 *Phys. Rev.* B **77** 85106
[15] Hedden R, Meden V, Pruschke T and Schönhammer K 2004 *J. Phys.: Condens. Matter* **16** 5279
[16] Karrasch C, Hedden R, Peters R, Pruschke T, Schönhammer K and Meden V 2008 *J. Phys.: Condens. Matter* **20** 345205
[17] Schütz F, Bartosch L and Kopietz P 2005 *Phys. Rev.* B **72** 035107
[18] Schütz F and Kopietz P 2006 *J. Phys. A: Math. Gen.* **39** 8205
[19] Kopietz P, Bartosch L and Schütz F 2009 *Lectures on the Renormalization Group—from the Foundations to the Functional Renormalization Group* (Berlin: Springer) at press
[20] Ledowski S and Kopietz P 2007 *Phys. Rev.* B **75** 045134
[21] Litim D F 2001 *Phys. Rev.* D **64** 105007
[22] Morris T R 1994 *Int. J. Mod. Phys.* A **9** 2411
[23] This result is implicitly contained in Tsvelick A M and Wiegmann P B 1983 *Adv. Phys.* **32** 453
[24] Hamann D R 1969 *Phys. Rev. Lett.* **23** 95
[25] Wang S Q, Evenson W E and Schrieffer J R 1969 *Phys. Rev. Lett.* **23** 92
[26] Castellani C and Di Castro C 1979 *Phys. Lett.* A **70** 37
[27] Schulz H J 1990 *Phys. Rev. Lett.* **65** 2462
[28] Macêdo C A and Coutinho-Filho M D 1991 *Phys. Rev.* B **43** 13515
[29] Dupuis N 2002 *Phys. Rev.* B **65** 245118
Borejsza K and Dupuis N 2003 *Europhys. Lett.* **63** 722
Dupuis N 2005 *Phys. Rev.* A **72** 013606
[30] Baier T, Bick E and Wetterich C 2004 *Phys. Rev.* B **70** 125111
Baier T, Bick E and Wetterich C 2005 *Phys. Lett.* B **605** 144
[31] Wetterich C 2007 *Phys. Rev.* B **75** 085102
[32] Strack P, Gersch R and Metzner W 2008 *Phys. Rev.* B **78** 014522